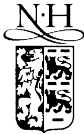

ELSEVIER

Nuclear Instruments and Methods in Physics Research B 175–177 (2001) 268–273

NIM B
Beam Interactions with Materials & Atoms

www.elsevier.nl/locate/nimb

Optical and structural properties of 6H–SiC implanted with silicon as a function of implantation dose and temperature

R. Héliou *, J.L. Brebner, S. Roorda

Laboratoire René-J.-A.-Lévesque, Université de Montreal, C.P. 6128, Succ. Centre-ville, Montréal, Qué., Canada H3C-3J7

Abstract

Optical and structural properties of ion-implanted 6H–SiC single crystals were investigated for samples implanted with 370 keV ^{28}Si ions to doses ranging from 5×10^{13} to 1×10^{16} cm^{-2} and at irradiation temperatures ranging from 20°C to 600°C. Rutherford backscattering spectrometry channeling (RBS/C) showed that dynamic recovery of the induced-damage layer increases with temperature. The final disorder determined from RBS/C as a function of implantation temperature was modeled in terms of a thermally activated process which yielded an activation energy of 0.08 eV. RBS/C data on high temperature implantations also suggest that defect complexes are created at high doses in addition to point defects still stable at high temperature. A decrease in Raman intensity of implanted samples relative to that of crystalline samples was observed and correlated with an increase in optical absorption near the wavelength of the laser pump (514.5 nm). © 2001 Elsevier Science B.V. All rights reserved.

PACS: 61.72.Ji; 61.72.Ww; 78.30.Am; 78.40.Fg
Keywords: Ion implantation; RBS; Raman; Absorption; Implantation temperature; SiC

1. Introduction

Due to its physical and electronic properties such as wide band gap, high breakdown electric field, high thermal conductivity and high saturated electron drift velocity, silicon carbide (SiC) has been widely studied in the last few years. It is a promising semiconductor material for high temperature, radiation resistant and high power/frequency electronic devices [1,2].

Dopant incorporation is a major step in electronic device fabrication. Due to low atomic mobilities in SiC, doping by thermal diffusion is not practical [3]. Clearly, ion implantation is an interesting alternative method provided the irradiation damage can be annealed out. A fundamental understanding of irradiation temperature dependence on residual implantation damage is necessary to use ion implantation effectively.

The aim of this paper is to investigate changes in the optical and structural properties of SiC as a

* Corresponding author. Tel.: +1-514-343-6111#4211; fax: +1-514-343-6215.
E-mail address: heliou@lps.umontreal (R. Héliou).

0168-583X/01/$ - see front matter © 2001 Elsevier Science B.V. All rights reserved.
PII: S0168-583X(00)00633-9

function of implantation dose and temperature. Rutherford backscattering spectrometry channeling (RBS/C), Raman spectroscopy and optical absorption were used to do so. Si was chosen as the implantation ion so that there would be no changes in the chemical structure of the SiC.

2. Experiment

Single crystal 6H–SiC wafers (from Cree Research), 250 μm thick, with (0 0 0 1) orientation were used. Damaged surface layers were produced by 370 keV Si^+ implantation with different doses (5×10^{13}–1×10^{16} Si^+/cm^2) and over a temperature range 20–600°C. The implantations were made at 7° off the [0 0 0 1] axis with a mean current of 1.5 μA raster scanned over an area of 1×1 cm^2. The energy of the implanted Si was chosen so the projected ion range (R_p) would be 370 nm [4], making the damaged layers easily accessible for RBS. The wafers were cut into 1×1 cm^2 pieces, each piece containing an irradiated and an unirradiated area. A total of 28 pieces of SiC were implanted at seven temperatures with four different doses for each temperature. These doses were chosen to be near the critical dose for amorphization without implanting more than 1% of Si in the SiC crystal.

RBS/C analysis was done with 2 MeV He^+ ions along the [0 0 0 1] channeling direction at a backscattering angle of 170°. The beam current was kept between 6 and 8 nA.

Raman spectra were recorded with a U1000 ISA double spectrometer coupled with a CCD camera cooled at LN_2. The 514.5 nm line of an argon ion laser was used in a backscattering geometry to observe Raman scattering. The laser intensity on the sample was ~40 mW focused on a 1×1 mm^2 region. Illumination was done perpendicular to the (0 0 0 1) plane but no effort was made to orient the sample with respect to the laser polarization.

The optical absorption measurements were done with a Perkin–Elmer Lambda 19 double spectrometer. The system is equipped with a halogen lamp (visible region) and a deuterium lamp (ultraviolet (UV) range) as light sources and a photomultiplier.

3. Results and discussion

3.1. RBS/C analysis

A set of typical RBS/C spectra obtained from samples implanted with 1×10^{15} Si^+/cm^2 at different temperatures are presented in Fig. 1. A spectrum of a randomly oriented virgin sample rotating around the [0 0 0 1] axis as well as a channeled spectrum along the same sample axis are also shown. Because the channeled backscattering yield reduction was more evident in the Si signal, all calculations of displaced atoms were performed on that part of the spectrum.

The ratio of channeled to random spectra near the surface was about 3%, thus showing the good single crystalline quality of the material. For each implanted sample, this ratio increased with dose but less so at higher implantation temperatures. The emergence of a damage peak in the channeling spectra indicates the presence of point defects which can cause direct backscattering of channeled ions and dechanneling. The distribution profile of these defects is not uniform, the maximum concentration varying in depth as a function of dose and temperature. The backscattering yield of the damaged layer reaches the random level only for the sample implanted with 1×10^{15} Si^+/cm^2 at room temperature (RT), hence this layer can be characterized as amorphous from a RBS/C viewpoint. This dose corresponds to 0.57 displacement per atom (dpa), as calculated from a Trim-97 simulation. Using TEM measurements, Zinkle and Snead [5] found the amorphization threshold for 560 keV Si^+ at RT to be 0.55 dpa. We therefore assume that the 1×10^{15} Si^+/cm^2 sample implanted at RT is truly amorphous and all other implanted samples are only partially damaged to different levels.

The thickness of the buried amorphous layer can be determined using the density of 6H–SiC (3.2 g/cm^3) and the energy width of the plateau region associated with the layer. The thickness is estimated to be ~440 nm. In the same way, we can calculate the depth at maximum value of the damage peak. This depth increases with implantation temperature to well beyond R_p. Furthermore, in samples implanted at 600°C at doses of

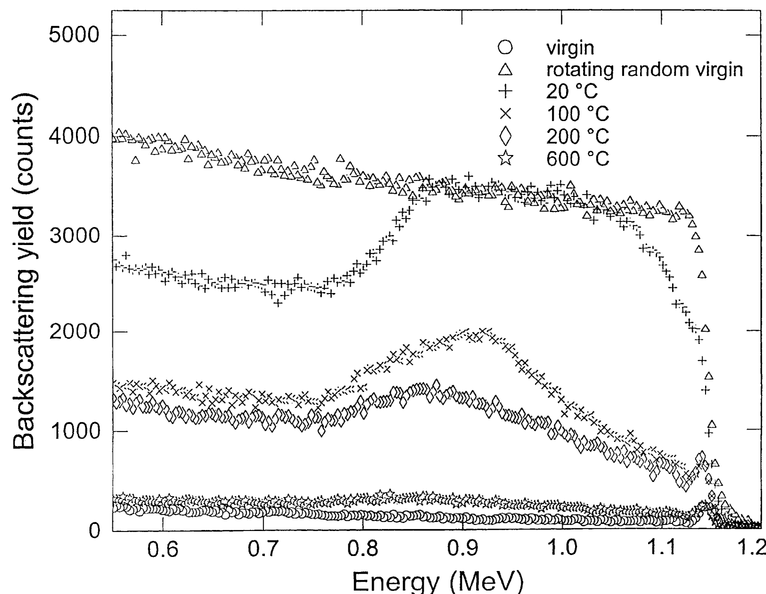

Fig. 1. Typical RBS/C spectra channeled in the [0 0 0 1] direction from virgin sample and samples implanted with 1×10^{15} Si^+/cm^2 at different temperatures. A random spectrum of a rotating virgin sample is also included.

5×10^{15} or 1×10^{16} Si/cm^2, defects are present at depths greater than the range accessible to 370 keV Si ions. These effects may be due to an increase in the diffusion length of the defects with temperature and also to the presence of the sample's surface which act as a trap, thus replacing the defect distribution to greater depths. At each implantation temperature (except RT), the depth at maximum value of the damage peak also increases with dose up to 5×10^{15} Si^+/cm^2. For all samples implanted with 1×10^{16} Si^+/cm^2 at temperatures of 200°C and higher, the shape of the channeled spectra appears to indicate the presence of two types of defects with overlapping distributions. The new distribution appears to be immobile and centered at R_p. We suggest that in addition to point defects still stable at these temperatures, there are defect complexes being created at high doses (and possibly high temperatures) significantly less mobile than the initial point defects.

The number of displaced Si (in atoms/cm^2) $N_d\Delta x$ in the crystal (representing the amount of disorder in the implanted layer) is determined from the area under the damage Si peak A_d relative to the random level near the surface H with the relation [6]

$$N_d\Delta x = (A_d \times \delta E)/(H \times [\varepsilon]), \quad (1)$$

where N_d is the displaced atoms density, Δx is the thickness of the damaged layer, δE is the energy width of a channel in the backscattered spectrum and $[\varepsilon]$ is the stopping cross section. A straight-line approximation is used to account for dechanneling.

These calculations reveal that all samples implanted at temperatures higher than RT exhibit a region where the disorder reaches a plateau at high doses (1×10^{15}–1×10^{16} Si^+/cm^2), the intensity at the plateau decreasing with increasing temperature. This plateau represents a saturation with ion dose of the quantity of defects still stable in the sample after implantation. The dynamic annealing generated by the heating process during implantation favors defect recombination by giving enough energy to interstitial atoms to migrate to an equilibrium position in the crystal. Even if no saturation is observed for RT implantations, high temperature implantation data suggest that a saturated level of disorder (in the same dose range as these implantations) could also be reached at higher doses for RT-implanted samples. The sat-

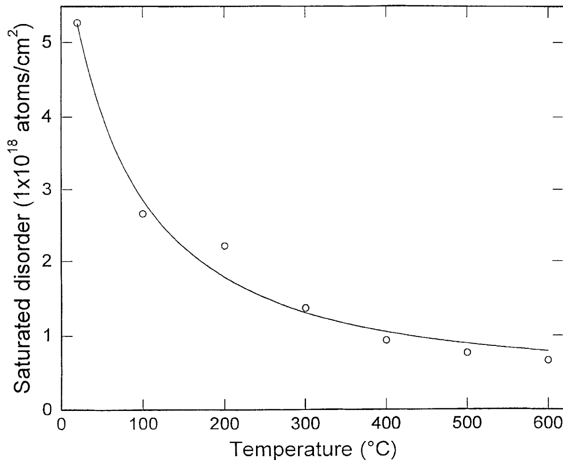

Fig. 2. Saturated disorder (in displaced Si atoms/cm^2) (as calculated from RBS/C spectra) as a function of implantation temperature. An Ahrrenius-type fit with an activation energy of 0.08 eV is included.

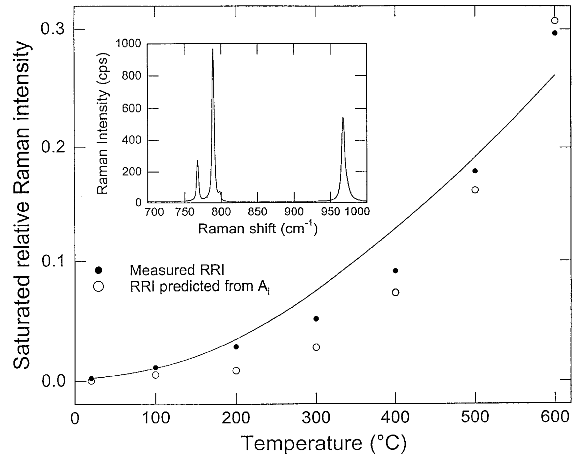

Fig. 3. Comparison of measured and predicted saturated relative Raman intensity as a function of implantation temperature. An Ahrrenius-type fit with an activation energy of 0.27 eV is included. Inset: Typical Raman spectrum of virgin 6H–SiC.

urated disorder (an average taken over all doses forming the plateau representing the disorder saturation) is plotted in Fig. 2 versus implantation temperature. An Arrhenius process fitted with an activation energy of 0.08 ± 0.01 eV is included in Fig. 2. This energy is interpreted as a migration energy and is in good agreement with the measured activation energies of Weber et al. [7].

3.2. Raman analysis

A Raman spectrum of virgin SiC is shown in the left corner of Fig. 3 where the Raman intensity is plotted versus the wave number shift with respect to the laser. Because the highest intensity Raman lines are located between 700 and 1000 cm^{-1}, all measurements were done in that range. Four sharp lines are observed at 768, 789, 797 and 967 cm^{-1}. The 768 and 797 cm^{-1} are, respectively, E_2 and E_1(TO) phonons. The 789 cm^{-1} line is either an E_2 or A_1(TO) while the 967 cm^{-1} is a combination of A_1(LO) and E_1(LO) vibration modes [8].

Raman spectra were taken on the implanted and unimplanted parts of each sample. No shift or broadening of the lines was observed. There was no evidence of other lines or bands appearing after implantation while no Raman signal was detected for the amorphous sample. However, a decrease in RRI with respect to the unirradiated part of the sample was observed and the lower the implantation temperature, the larger the reduction in RRI. This suggests that the Raman signal mainly comes from the crystalline substrate underneath the implanted layers.

The relative Raman intensity (RRI) as a function of implantation dose for different implantation temperatures is also calculated. Here RRI means Raman intensity of implanted sample divided by Raman intensity of unimplanted part of the same sample averaged over the three more intense lines (768, 789 and 967 cm^{-1}). At low doses, the RRI decreases monotonically only to saturate at higher doses. The saturated RRIs (calculated by taking an average over all doses forming the plateau regions) are shown in Fig. 3 as a function of implantation temperature. We see that the saturated RRI increases exponentially with temperature and that it tends to zero at low temperatures and possibly to one at higher temperatures. The data seem to be of an Arrhenius-type, but the fitting procedure gives a poorly defined activation energy and we can only conclude that the latter is less than 0.27 eV. As shown below, the loss in Raman signal is due to increased optical absorption in the damaged layers.

3.3. Optical absorption

The level of damage in the implanted samples was also followed by optical absorption in the UV and visible range. For each sample, a ratio I/I_0 was measured as a function of the wavelength (between 200 and 860 nm), where I is the intensity of the transmitted light and I_0 is the intensity of the incident beam. From the implanted and virgin measured I/I_0 ratios and Beer's Law, we can deduce the induced absorbance of the implanted layer (A_i) which is defined as the absorption coefficient of the damaged layer (α_i) times the thickness of the layer. Reflectance values of unimplanted ($R_c = 0.2$) and amorphous ($R_a = 0.28$) samples are based on the work of Musumeci et al. [9] while all other implanted samples have an intermediate reflectance $R_i = R_c + (A_i/A_a)(R_a - R_c)$, where A_a is the absorbance of the amorphous sample.

A large absorption band is detected following implantation due to defect-related energy levels in the gap. The absorption increases with dose for constant temperature but again seems to be independent of dose at higher temperature. As temperature increases, the absorption band becomes narrower, the band curvature is more abrupt and the position of maximum absorption shifts towards higher energies.

To compare absorption and Raman measurements, we have calculated A_i at the laser wavelength used for Raman spectroscopy (514.5 nm). For low doses, A_i increases monotonically and then saturates at a certain dose ($>1 \times 10^{15}$ cm^{-2}) in the same way as RBS disorder or RRI. We can see more easily the effect of implantation temperature by calculating the saturated A_i level at 514.5 nm. The decrease in absorption is linear with temperature for damaged layers while the RT implantation is a special case because of its amorphous state.

This data can also be used to correlate the decrease in intensity of the Raman signal in the implanted samples. If we assume: (1) that the Raman signal is originating from the crystalline part of the sample; (2) that the quantity of crystalline material probed by the laser beam in unimplanted and implanted samples is almost identical (an implanted layer of 0.37 μm over a total thickness of 250 μm); (3) that the loss in Raman signal is only caused by a reduction in intensity of the laser beam due to optical absorption in the implanted layer; then the RRI should be related to A_i according to

$$I_i/I_c = ((1 - R_i)/(1 - R_c))^2 \exp(-2A_i), \qquad (2)$$

where I_i is the RRI of an implanted sample and I_c is the RRI of an virgin sample. The factor 2 originates from the reduction of the beam intensity by a factor $\exp(-A_i)$ when it traverses the implanted layer and another factor $\exp(-A_i)$ when it goes out of the sample to the detector. We can predict the ratio I_i/I_c with Eq. (2) and A_i measurements and compare this ratio to our Raman measurements. The results are shown in Fig. 3. We see that predicted I_i/I_c ratio fits well with the data although it slightly underestimates actual RRIs. This is probably due to partial contribution of the implanted layer to the Raman signal and an overestimation of A_i due to light diffusion by defects.

4. Conclusions

Residual damage in 6H–SiC single crystals after implantation at different temperatures has been followed by RBS/C, Raman spectroscopy and optical absorption.

Disorder calculations indicate damage recovery during implantation with an activation energy of 0.08 ± 0.01 eV. RBS/C data on high temperature implantations also suggest that for doses of 1×10^{16} Si^+/cm^2, defect complexes are created in addition to point defects still stable at high temperature. The diffusion process of these two types of defects is however different.

Optical absorption measurements have been used to correlate the decrease in relative RRI as a function of temperature with an increase in absorbance of the damaged layer.

Acknowledgements

The authors would like to thank P. Berichon and R. Gosselin for their help with the Tandetron accelerator and F. Schiettekatte, M. Chicoine, A. Tchebotareva and R. Poirier for many fruitful

discussions. This research was supported by the Natural Sciences and Engineering Research Council of Canada (NSERC) and Le Fonds pour la Formation de Chercheurs et l'Aide à la Recherche (FCAR).

References

[1] V.E. Celnokov, Mater. Sci. Eng. B 11 (1992) 103.
[2] K. Shnai, R.S. Scott, B.J. Baliga, IEEE Trans. Electron Devices 36 (1989) 1811.
[3] R.F. Davis, G. Kelner, M. Shur, J.W. Palmour, J.A. Edmond, Proc. IEEE 79 (1991) 677.
[4] J. F Ziegler, J.P. Biersack, in: The Stopping and Range of Ions in Solids, Pergamon, New York, 1985.
[5] S.J. Zinkle, L.L. Snead, Nucl. Instr. and Meth. B 116 (1996) 92.
[6] M.L. Swanson, in: J.R. Tesmer, M. Nastasi (Eds.), Handbook of Modern Ion Beam Materials Analysis, MRS, Pittsburgh, 1995, p. 271.
[7] W.J. Weber, L.M. Wang, N. Yu, N.J. Ness, Mater. Sci. Eng. A 253 (1998) 62.
[8] D.W. Feldman, J.H. Parker, W.J. Choyke, L. Patrick, Phys. Rev. 170 (1968) 698.
[9] P. Musumeci, L. Calcagno, M.G. Grimaldi, G. Foti, Nucl. Instr. and Meth. B 116 (1996) 327.